SIMULATING VENTED HYDROGEN DEFLAGRATIONS: IMPROVED MODELLING IN THE CFD TOOL FLACS-HYDROGEN

Lucas, M.[1,2], Atanga, G.[1], Hisken, H.[1], Mauri, L.[1]and Skjold, T.[2]
[1] Gexcon AS, Fantoftvegen 38, 5072 Bergen, Norway, melodia@gexcon.com
[2] Department of Physics and Technology, University of Bergen, Allégaten 55, 5007 Bergen

ABSTRACT

This paper describes validation of the computational fluid dynamics tool FLACS-Hydrogen. The validation study focuses on concentration and pressure data from vented deflagration experiments performed in 20-foot shipping containers as part of the project *Improving hydrogen safety for energy applications through pre-normative research on vented deflagrations* (HySEA), funded by the Fuel Cells and Hydrogen Joint Undertaking (FCH 2 JU). The paper presents results for tests involving inhomogeneous hydrogen-air clouds generated from realistic releases performed during the HySEA project. For both experiments and simulations, the peak overpressures obtained for the stratified mixtures are higher than those measured for lean homogeneous mixtures with the same amount of hydrogen. Using an in-house version of FLACS-Hydrogen with the numerical solver Flacs3 and improved physics models results in significantly improved predictions of the peak overpressures, compared to the predictions by the standard Flacs2 solver. The paper includes suggestions for further improvements to the model system.

Keywords: hydrogen safety, stratified hydrogen mixtures, computational fluid dynamics, vented hydrogen deflagrations, combustion model

1. INTRODUCTION

Accidental releases and ignition of hydrogen-air mixtures in confined spaces represent a significant hazard for many hydrogen energy applications. Explosion venting is a common measure to mitigate the consequences of gas explosions in enclosures. International standards, such as EN 14994 [1] and NFPA 68 [2], describe basic design requirements for deflagration venting devices. The empirical and semi-empirical models used are mostly based in experiments performed in empty enclosures. However, for most low-strength enclosures where an accidental release of hydrogen may occur, internal congestion is unavoidable. This includes buildings and containers at hydrogen refuelling stations, as well as fuel preparation and fuel cell rooms in ships fuelled by hydrogen. It is inherently difficult to capture the effect of congestion on flame acceleration and pressure build-up in empirical or semi-empirical correlations. Expansion-generated turbulent flow in wakes behind obstacles, increased flame surface area caused by flame folding, and geometry-induced flame instabilities may all contribute to an overall increase in the rate of combustion. Furthermore, most empirical and semi-empirical models do not account for the effect of stratification that typically will occur after spills of liquified or gaseous hydrogen in an enclosed space.

In principle, computational fluid dynamics (CFD) simulations can account for the effect of stratification in the flammable clouds, as well as the effect of obstacles and the presence of vent panels, on the flame acceleration and overpressure generated in vented deflagrations. However, for risk assessments in industry, it is necessary to estimate the consequences of numerous large-scale scenarios within a limited time frame. For such applications, it is not possible to resolve all relevant spatial and temporal scales of the physical phenomena involved. To obtain sufficiently accurate predictions, while retaining acceptable simulation times, several commercial simulation tools rely on the so-called porosity/distributed resistance (PDR) concept. Within the PDR framework, sub-grid geometry is represented as area and volume porosities (denoting the degree of "openness" for each grid cell). This paper summarises the results from a validation study that was undertaken for the in-house developed numerical solver Flacs3, which includes updated sub-grid models for premixed combustion [3]. The empirical data comprises the

vented deflagration experiments performed in 20-foot shipping containers and presented as part of the second blind prediction benchmark study in the framework of the HySEA project [4]. The HySEA project was funded by the Fuel Cells and Hydrogen 2 Joint Undertaking. The discussion highlights the predictive capabilities and inherent limitations of the model system.

2. FLACS-HYDROGEN

FLACS-Hydrogen is a module of the CFD tool FLACS [3] for hydrogen safety applications that was first developed in connection with the Network of Excellence (NoE) HySafe, funded by the European Commission. The model has since been developed through several R&D projects at Gexcon and is continually validated for hydrogen applications.

This paper compares two versions of FLACS-Hydrogen: FLACS *v10.9* (released in 2019) and FLACS *v11 beta* (released as a beta version together with FLACS *v10.9*). The Flacs2 solver, which is used in the commercial release FLACS *v10.9*, is replaced by the Flacs3 solver in the FLACS *v11 beta* version. Both Flacs2 and Flacs3 are PDR solvers that apply the SIMPLE numerical technique to handle the pressure-velocity coupling. The governing equations are discretized on a structured Cartesian mesh [5, 6]. In Flacs2, the pre-processor *Porcalc* computes the area and volume porosities. In Flacs3, the FLACS Geometry Calculator (FGC) replaced *Porcalc*. In addition to porosities, FGC calculates the geometrical length scale (*GLS*) used by the combustion model. Both solvers use a first-order backward Euler scheme controlled by Courant–Friedrichs–Lewy (CFL) numbers for time-stepping.

Both Flacs2 and Flacs3 include additional terms for representing turbulence generation by flow past sub-grid objects, a combustion model based on the flamelet approach, and a numerical flame model that applies an artificially thickened flame front [7]. The next sections outline the main differences in the modelling approaches between Flacs2 (FLACS *v10.9)* and Flacs3 (FLACS *v11 beta)*.

2.1 Turbulence modelling

Both solvers use the standard *k-ε* model [8] adopted for the PDR concept:

$$\frac{\partial}{\partial t}(\beta_v \rho k) + \frac{\partial}{\partial x_i}(\beta_j \rho u_i k) = \beta_v P_k - \beta_v \rho \varepsilon + \frac{\partial}{\partial x_i}\left[\beta_j \frac{\mu_{eff}}{\sigma_k}\frac{\partial k}{\partial x_i}\right] \quad \text{and} \tag{1}$$

$$\frac{\partial}{\partial t}(\beta_v \rho \varepsilon) + \frac{\partial}{\partial x_i}(\beta_j \rho u_i \varepsilon) = \beta_v P_\varepsilon - \beta_v C_{2\varepsilon} \rho \frac{\varepsilon^2}{k} + \frac{\partial}{\partial x_i}\left[\beta_j \frac{\mu_{eff}}{\sigma_\varepsilon}\frac{\partial \varepsilon}{\partial x_i}\right], \tag{2}$$

where β_v and β_j are the volume and the surface area porosities, respectively, ρ is the density, k is the turbulence kinetic energy, u_i is the velocity in the i^{th} direction, P_k is the production of turbulence kinetic energy, ε is the dissipation rate of turbulence kinetic energy, μ_{eff} is the effective dynamic viscosity, P_ε is the production of dissipation rate of turbulence kinetic energy, and $C_{2\varepsilon}$, σ_k and σ_ε are model constants.

2.2 Combustion modelling

The model for premixed combustion in both Flacs2 and Flacs3 consists of

- a numerical flame model,
- a burning velocity correlation model,
- a combustion length-scale model, and
- a flame wrinkling model.

These components are briefly described below, highlighting differences and similarities between the two solvers.

2.2.1 The numerical flame model

In the present work, the same numerical flame model is used in both solvers. The conservation equation for the fuel mass fraction Y_F is expressed as:

$$\frac{\partial}{\partial t}(\beta_v \rho Y_F) + \frac{\partial}{\partial x_j}(\beta_j \rho u_j Y_F) = \frac{\partial}{\partial x_j}\left(\beta_j \rho D \frac{\partial Y_F}{\partial x_j}\right) + R_F. \quad (7)$$

Here, the diffusion coefficient, D, and the chemical reaction source term, R_F, are expressed as:

$$D = C_{\beta D}\, s\Delta \text{ , and} \quad (8)$$

$$R_F = C_{\beta R_F} \frac{S}{\Delta} \rho \min\left(1 - \frac{Y_F}{Y_{F0}}, 9\frac{Y_F}{Y_{F0}}\right) \quad (9)$$

where $C_{\beta D}$ and $C_{\beta RF}$ are model constants, s is the burning velocity, Δ is the control volume length in the direction of flame propagation, and Y_{Fo} is the initial fuel mass fraction.

2.2.2 Burning velocity correlations

Correlations for the burning velocity are provided for different mixtures and flow regimes. The laminar burning velocity in both solvers, which is input to the burning velocity in all flow regimes, depends on the pressure as [7]:

$$s_L = s_{L0}\left(\frac{P}{P_0}\right)^{\gamma}, \quad (11)$$

where s_{L0} is the laminar burning velocity at atmospheric pressure, P_0, P is the pressure, and γ is a fuel dependent parameter. To model the regime of cellular flame propagation, both solvers use the quasi-laminar burning velocity concept. In Flacs2, the quasi-laminar burning velocity is modelled as

$$s_{QL} = s_L\left(1 + C_{QL} r_F{}^a\right), \quad (12)$$

where s_{QL} is the quasi-laminar burning velocity, C_{QL} is a mixture-dependent model constant, r_F is the flame radius, and a is a model constant. In Flacs3, the burning velocity in the quasi-laminar regime is given as

$$s_{QL} = s_L C^*_{QL}\left(\frac{r_F}{r_{F,cr}}\right)^{a^*}, \quad (13)$$

where $r_{F,cr}$ denotes the critical radius of the appearance of a cellular flame, and the model constants C^*_{QL} and a^* are both concentration- and mixture-dependent.

For the turbulent regime, a Markstein number-dependent burning velocity model is implemented in the Flacs3 solver. The turbulent burning velocity, S_T, is expressed in terms of the effective root-mean-square turbulence velocity, u_k', and the Karlovitz stretch factor K [9] as:

$$\frac{s_T}{u'_k} = \alpha K^{-\beta}, \qquad K = 0.25\left(\frac{u'}{s_L}\right)^2\left(\frac{u' l_C}{\upsilon}\right)^{-0.5}, \quad (14)$$

where u' is the turbulence velocity, υ is the kinematic viscosity, l_C is the combustion length scale, and α and β are empirical parameters explicitly expressed in terms of the strain rate Markstein number. Thus, the variation in reactivity between various fuels and concentrations, including the response of the burning rate to varying flow properties, is accounted for when predicting the turbulent burning velocity. Flacs2 applies the turbulent burning velocity correlation proposed by Bray [10], which is on the same form as Equation (14) with fixed values for α and β. This correlation only accounts for differences in reactivity between various mixtures and concentrations through the laminar burning velocity. Quenching of the turbulent flame is limited by $K = 1$ in Flacs2 and $K = 10$ in Flacs3. The low intensity turbulent burning velocity correlation for both solvers [7] is:

$$s_T = 0.96\, u'^{0.912} s_L{}^{0.284} l_C{}^{0.196} \nu^{-0.196} + s_L. \quad (15)$$

According to Lipatnikov and Chomiak [11], s_T should increase with increasing pressure, despite the corresponding decrease in s_L. For the correlation described by Bradley *et al.* [9], this effect can be included through a pressure dependent Markstein number *Ma* and the kinematic viscosity υ. In Flacs3, the turbulent burning velocity varies with pressure according to the expression:

$$s_T^p = s_T \left(\frac{P}{P_0}\right)^b \tag{16}$$

where b is a model constant that has been fitted to match experimental measurements, and P_0 is a reference pressure. This correction is not applied in Flacs2.

2.2.3 Combustion length scale model

In Flacs2, the local turbulence length scale l_C used by the turbulent burning velocity correlation is proportional to the distance from the point of ignition to the flame front. For confined geometries, this growth is bounded by a parameter that is proportional to the distance between the enclosing walls. This simple model works reasonably well for single module configurations and many confined scenarios, but can result in unphysical results for flame propagation in unconfined and congested regions of high aspect ratio. In Flacs3, for grid cells with sub-grid obstructions the combustion length scale is determined by a characteristic geometrical length scale of the sub-grid congestion, *GLS*. For uncongested grid cells, the current model system uses a simple combustion length scale model based on a wall distance formulation that decouples the resulting length scale from the employed turbulence model.

2.2.4 Flame wrinkling model

The flame wrinkling model accounts for the increase in the burning velocity due to the flame surface area increase generated by sub-grid obstructions. A common approach for modelling flame folding due to sub-grid obstacles and flame instabilities entails the use of a transport equation [12, 13]. This approach is adopted in Flacs3 which solves a transport equation for the relative increase in flame surface area generated by the interaction with sub-grid obstacles based on the modelling approaches presented by Weller *et al.* [14] and Puttock *et al.* [15]:

$$\frac{\partial}{\partial t}(\rho\Xi_s) + \frac{\partial}{\partial x_i}(\rho u_i \Xi_s) = \rho G_s \Xi_s - \rho R_s(\Xi_s - 1), \tag{17}$$

where Ξ_s is the flame wrinkling factor, and G_s and R_s are the generation and removal rates of Ξ_s, respectively. Flacs2 uses an equilibrium expression to represent this effect [7].

3. THE EXPERIMENTAL PROGRAMME

As part of the HySEA project [16], Gexcon performed 66 vented deflagration tests in 20-foot ISO containers [17]. The first experimental campaign involved homogenous hydrogen clouds with different concentration and different obstructions inside the container. The second experimental campaign involved release of hydrogen in the container at different flow rates using a circular pipe of 18 mm diameter (jet release) or a 200 mm square box (diffusive release).

Table 1 summarises the experimental configurations of the tests used for this validation study. Tests 57, 59, 60 and 61 were part of the second blind-prediction of the HySEA project [4]. For comparison of the effects of having homogeneous vs. stratified clouds, as well as diffusive releases vs. jet releases, tests 41, 44 and 46 are included in the validation study. The flow rate for the tests with stratified clouds was 56 m^3/h and the release was terminated after 450 s to achieve a nominal fuel concentration of 21% inside the container. The stratified mixtures were ignited at the back wall, about 2 m above the container floor, 30 s after the end of the release. The container roof had six openings that were covered with commercial pressure relief panels (6P). The geometry inside the containers was either only the frame on the floor used to support obstacles (FO), or a pipe rack fixed to the frame in centre position (P2). Skjold et al. [18, 17] describe the experimental setup in detail.

Table 1. Experimental configurations.

Test	Configuration	Release	Duration (s)	Flow rate (m^3/h)	Venting
T41	FO	Diffusive	450	56	*
T44	FO	Diffusive	450	56	6P
T46	P2	**	**	**	6P
T57	FO	Jet	450	56	6P
T59	FO	Jet	450	56	6P
T60	P2	Jet	450	56	6P
T61	P2	Jet	450	56	6P

*Unignited test
** Reference test with homogeneous mixture

4. MODEL SETUP

Figure 1 illustrates the geometry model used for simulations for the container with the pipe rack together with the location of the monitor points. The monitor points A4, B4, C4, D4 and E4 represent low-cost sensors that measured the oxygen concentration continuously during the experiments. A Servomex Xendos 2223 analyser measured the oxygen concentration in samples collected from points A4', B4', C4', D4' and E4' (not shown) located at the same vertical levels as A4-E4, respectively, and at a horizontal distance of 2.2 m. The pressure sensors P1, P3, P5 and P7 (yellow font) are symmetrically arranged with respect to sensors P2, P4, P6 and P8 (not shown).

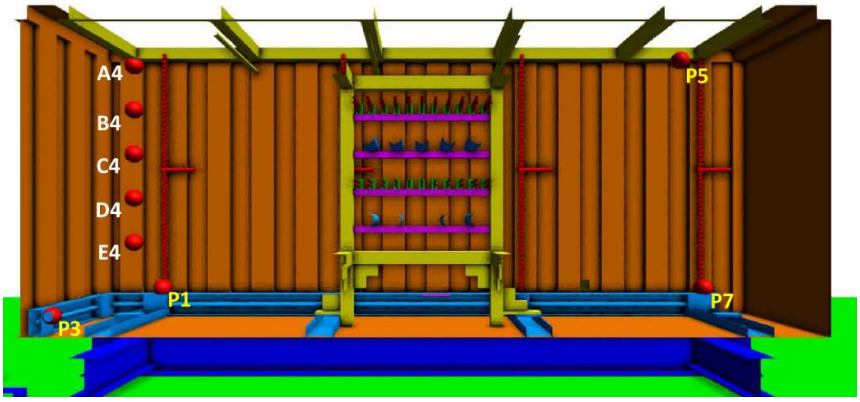

Figure 1. Vertical cross section of geometry model for the container with the pipe rack in centre position.

The width of the square pipes in the frame that supported the vent panels on the container roof was 10 cm. This implies that the maximum grid size that facilitates aligning the panels with the grid is 10 cm [3]. Figure 2 shows the pressure-time histories from simulations with Flacs3, performed with two grid resolutions: 5 and 10 cm. The peak pressures do not vary significantly, compared to the variation in measured peak pressure for the repeated experiments (tests 46 and 47). All results presented in the following were obtained with a grid resolution of 10 cm.

Guidelines for grid refinement around the leak points were followed for all dispersion simulations [3]. The CFLC number was set to 125 for the jet leaks, and 80 for diffusive leaks, to reduce the effect of local grid refinement on the time step. The results obtained from the dispersion simulations were used as input to the explosion simulations. Here, the CFLC and CFLV numbers were set to 5 and 0.5, respectively.

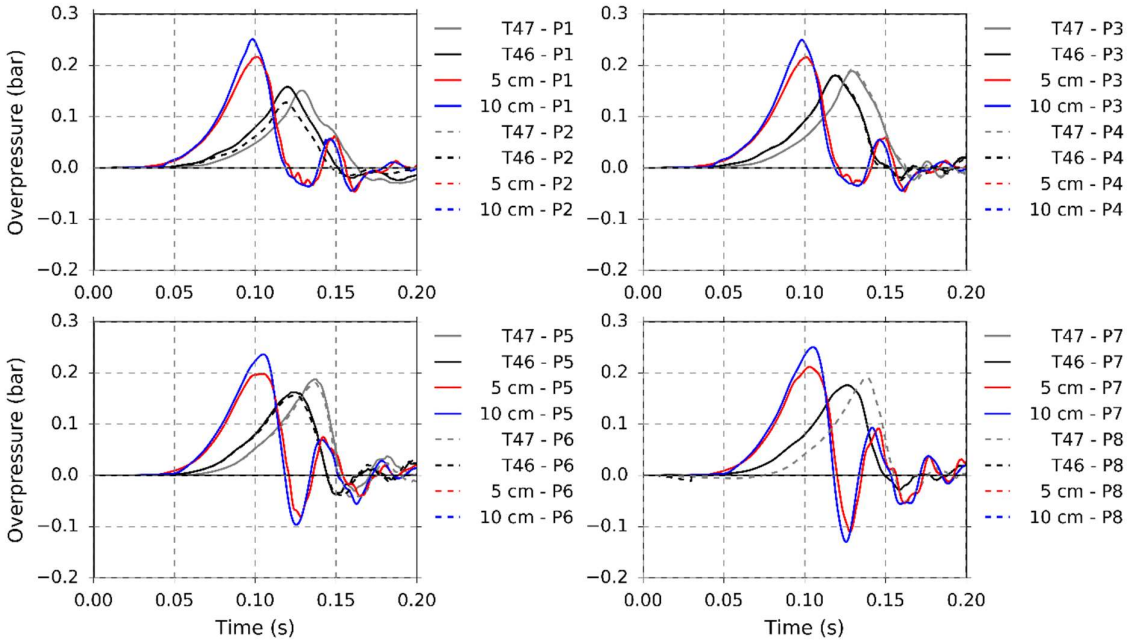

Figure 2. Example of grid sensitivity of the Flacs3 solver for a homogenous cloud test.

The commercial vent panels were modelled as hinged panels with specific weight 6.8 kg/m^2 and opening pressure 100 mbar. The vent panels in FLACS are represented by porosities that vary gradually from 0 (fully blocked) to 1 (fully open) at the panel location. The porosity at each control volume face covered by the panel depends on the pressure forces applied at each control volume face.

5. RESULTS AND DISCUSSION

Figure 3 and Figure 4 show the comparison of the predicted hydrogen concentration with experimental data for sensors A4-E4 and A4'-E4'. The experimental results are labelled with a T followed by the test number (i.e. T57 corresponds to Test 57), cf. Table 1. The measurements in A4-E4 for the first test are represented by dashed lines and the A4'-E4' by square dots. The results from the repeated tests are represented by dotted lines and diamonds. The predicted hydrogen concentrations from both Flacs2 and Flacs3 are exactly overlapping in Figure 3 and Figure 4, since the models for dispersion in both solvers are identical. Therefore, only the Flacs3 results are plotted for the dispersion simulations, represented by solid lines. The vertical lines indicate the end of the release and the time of ignition.

FLACS reproduces the stratification observed in the experiments reasonably well. A slightly lower concentration of hydrogen was measured for test 57, 59 and 60 than for the corresponding unignited experiments with the same release characteristics (tests 42 and 39 in [4]), which might have been caused by the deformation of the container from earlier tests and the initial offset of the flow rate in these tests [4]. For the monitor point E4, the concentration at the time of ignition for Test 57 was about 2.3 vol.% lower than for the corresponding unignited test (Test 42 in [4]). Also, the concentration measured by the Servomex analyser differed from the concentration measured by the continuous measurement at monitor points D4 and E4, in particular for Test 59. Loss of hydrogen from small openings in the container and somewhat increased volume of the container due to deformation may explain the over-prediction of hydrogen concentrations observed in the simulations.

FLACS reproduces the clouds generated by the area release from the box better than the clouds generated by the jet release. The diffuse leak in FLACS applies the surrounding flow velocity to the leaking gas. However, for the jet leak, the temperature of the outflow is used to obtain the velocity of the outflow. This assumption introduces additional uncertainty to the modelling. Given that the standard

k-ε model is known for overestimating the spreading rate of turbulent round jets, a FLACS simulation of the jet leak in the empty container was attempted using the model modification proposed by Morse [19] and Pope [20], with $C_{1\varepsilon} = 1.6$ (instead of $C_{1\varepsilon} = 1.44$, as in the standard *k-ε* model adopted by default in FLACS). The Flacs3 simulations with the modified $C_{1\varepsilon}$ constant overpredicted the concentration at time of ignition at points A4, B4 and C4 with a concentration 5% higher than with the standard Flacs3 simulations. At point D4, the concentration was similar for both turbulence models and at point E4 the modified version of Flacs3 predicted lower concentration than the standard version. Overall, the concentration prediction did not improve when setting $C_{1\varepsilon}$ to 1.6 in the turbulence model. The increased $C_{1\varepsilon}$ value in the modified model version determined increased dissipation rate of turbulent kinetic energy and thus decreased diffusivity leading to a more pronounced stratification of the hydrogen in the container, compared to the standard model and to experiments.

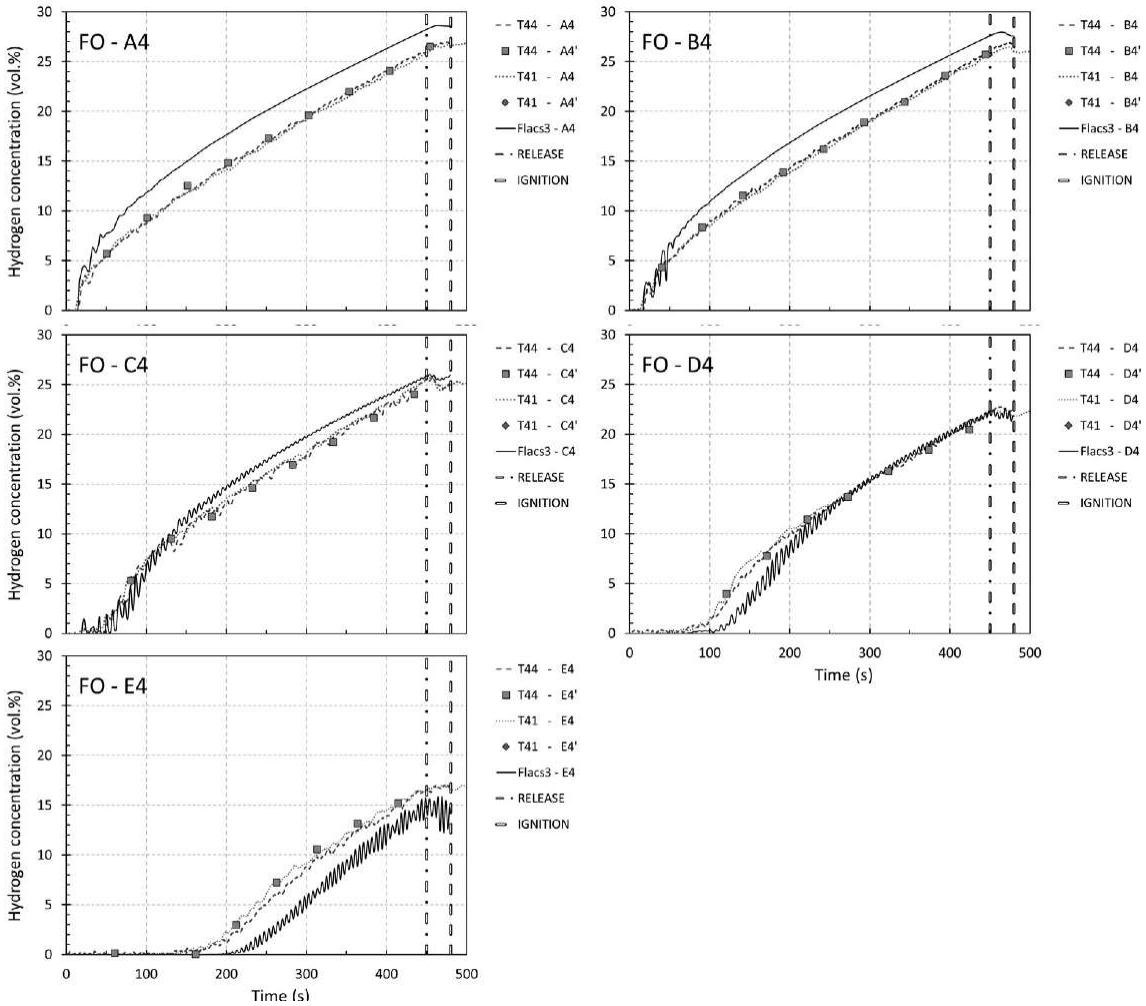

Figure 3. Hydrogen concentrations for hydrogen diffusive releases in the empty container (FO).

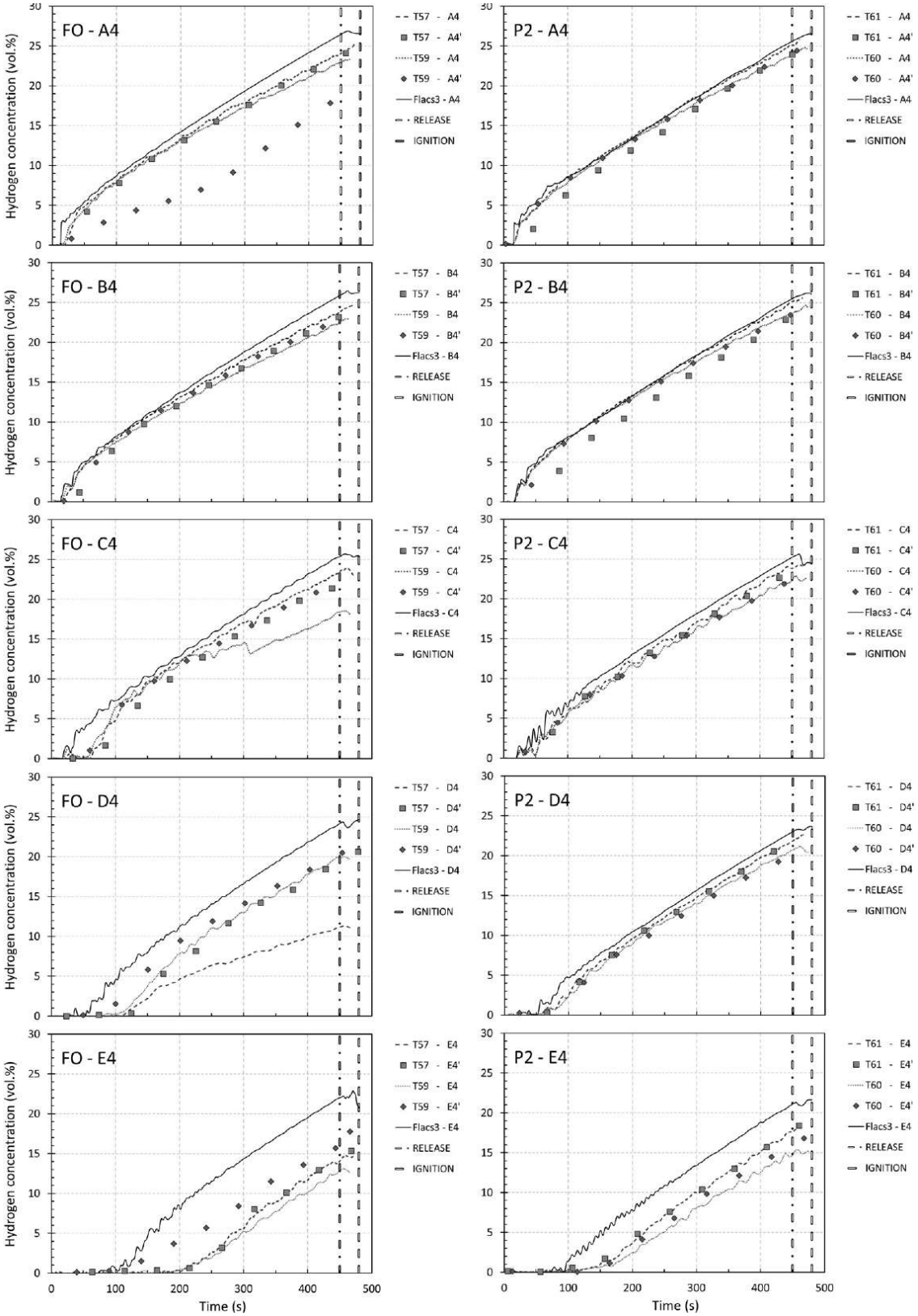

Figure 4. Hydrogen concentrations for hydrogen jet releases for both scenarios (FO and P2).

Table 2 summarises the results for the explosion simulations. The maximum overpressures from the first experiment and the repetition, if any, are shown together with the predicted maximum overpressure by Flacs2 and Flacs3. The description of the case in Table 2 indicates the obstacles in the container (P2 or FO), the venting (6P), the leak source (jet or leak), the average hydrogen concentration and whether the mixture in the container was homogeneous or inhomogeneous. For tests 57 and 59, the panel opening pressure (estimated from video recordings), was found to be about 80 mbar (rather than 100 mbar). Additional simulations with Flacs3 with panel opening pressures of 80 mbar resulted in a reduction in predicted peak overpressure of about a 100 mbar.

Table 2. Summary of maximum peak overpressures.

Case	Maximum peak overpressure (bar)			
	Flacs2	Flacs3	Experiment	Repetition
P2, 6P, Jet, 21 % Inhomogeneous	11.53	1.12	(T60) 0.37	(T61) 0.68
FO, 6P, Jet, 21 % Inhomogeneous	6.55	0.80 / 0.70[a]	(T57) 0.34	(T59) 0.34
FO, 6P, 21 % Homogeneous	0.60	0.25	(T46) 0.19	(T47) 0.20
FO, 6P, Diffusive, 21 % Inhomogeneous	4.37	0.79	(T44) 0.41	-

[a] **Simulation with panel opening pressure 80 mbar**

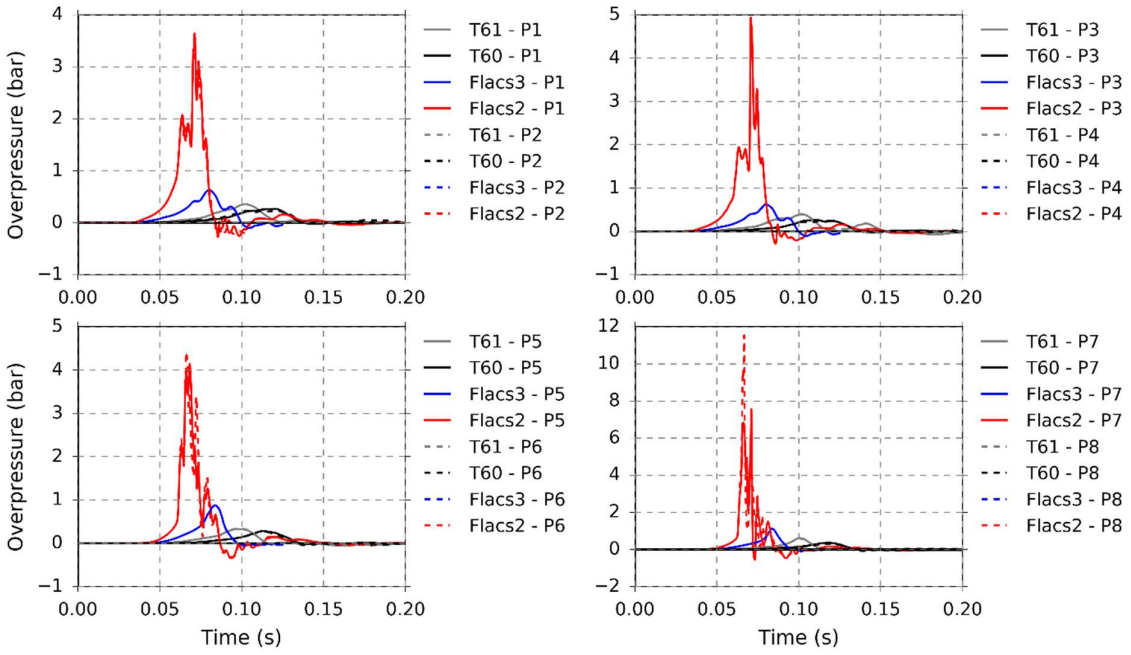

Figure 5. Predicted pressure-time histories and experimental results for tests with a jet release of hydrogen, commercial vent panels and a pipe rack inserted in the container.

Figure 5, Figure 6 and Figure 7 show the overpressure-time curves for the tests with stratified hydrogen mixtures in the container. The experimental results are represented by black and grey lines. The Flacs2 results are represented by red lines and Flacs3 results by blue lines. The monitor points P1, P3, P5 and P7 are represented by solid lines and their symmetric counterparts (P2, P4, P6 and P8, respectively) by dashed lines. Figure 5 and Figure 6 show the overpressure-time histories for the tests with the 450 s release from the pipe, using six commercial vent panels. Tests 60 and 61 were performed with a pipe rack inside the container. Figure 7 shows the overpressure recorded for Test 44, with ignition after 450 s of a 56 m^3/h diffusive hydrogen release and with a pipe rack inside the container.

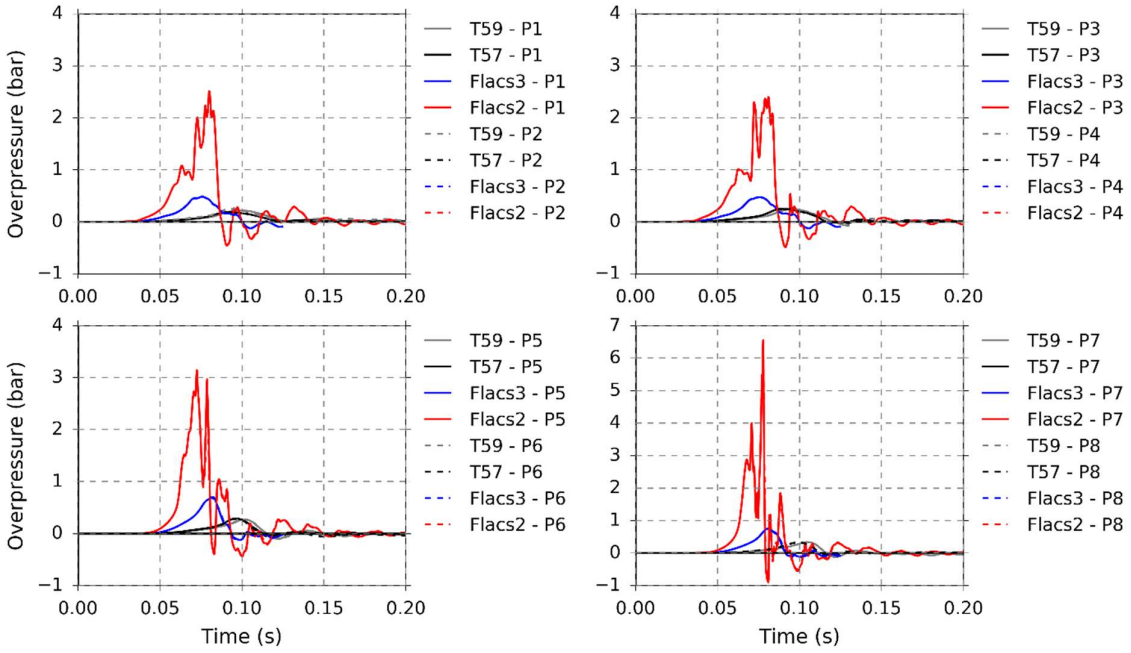

Figure 6. Predicted pressure-time histories and experimental results for tests with a jet release of hydrogen, commercial vent panels and only the frame inserted in the container.

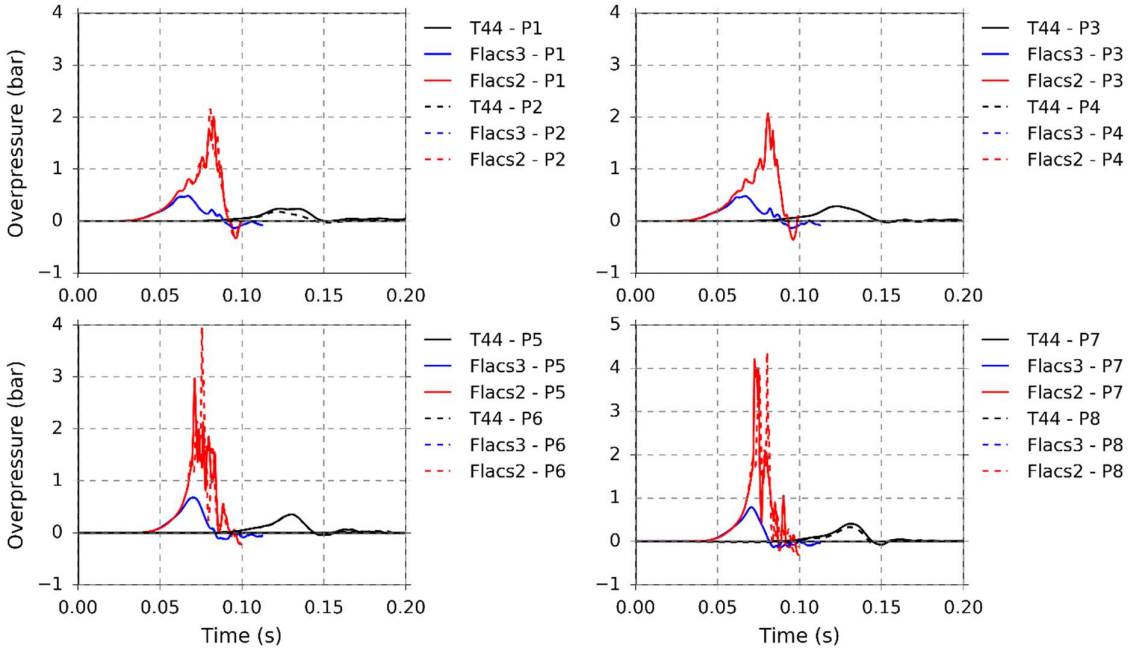

Figure 7. Predicted pressure-time histories and experimental results for tests with a diffusive release of hydrogen, commercial vent panels and only the frame inserted in the container.

As presented in Table 2, Figure 5 and Figure 6, the significant over-prediction of explosion overpressure by FLACS *v10.9* and FLACS *v10.8* (using the Flacs2 solver and presented in the second blind-prediction of the HySEA project [4]) is considerably reduced in simulations with FLACS *v11 beta* (using the Flacs3 solver).

Figure 8 shows the flame speed for simulations representing the scenario in tests 60 and 61. The flame speed was calculated using the distance from the ignition point to the location of the 1200 K isotherm.

Figure 8 shows that from the time of ignition, the flame speed predicted by Flacs2 is higher than that predicted by Flacs3. In the early phase of flame propagation, before the flame front reaches the pipe rack, the quasi-laminar burning velocity governs the flame propagation for both FLACS versions. For tests 60 and 61, in the region before the pipe rack, the quasi-laminar burning velocity predicted by Flacs2 is about 2 m/s higher than that predicted by Flacs3. Once the flame enters the congestion region, the flame acceleration is significantly higher for Flacs2 than for Flacs3. Here, both the flame folding due to sub-grid obstructions and the turbulent burning velocity models in the two solvers are different. The turbulent burning velocity model in Flacs2 predicts a burning velocity at the time of peak pressure that is considerably higher than the model in Flacs3.

For hydrogen-air mixtures, Flacs2 applies a Lewis number dependent correction directly to the laminar burning velocity [21], resulting in an enhancement in the laminar burning velocity for lean mixtures and a reduction in the laminar burning velocity for rich mixtures [22]. This correction thus accounts for Lewis (or Markstein) number dependent effects for hydrogen-air flames in all flow regimes, and most likely contributes to the over-prediction of the reactivity of lean hydrogen-air mixtures with a fuel concentration ranging from around 18-24 vol% [22, 23]. Meanwhile, Flacs3 accounts for Lewis/Markstein-number dependent effects for each regime of flame propagation separately. Overall, Flacs2 predicts higher values for the laminar and quasi-laminar burning velocities than Flacs3 for hydrogen-air mixtures in the concentration range involved in these tests. The model for the combustion length scale in Flacs2 also yields higher values for the turbulence combustion length scale l_C, which is used as input to the turbulent burning velocity correlation.

The occurrence of the maximum overpressure takes place earlier in the simulations than in the experiments for both solvers. The ignition process itself is not accurately modelled in FLACS, so the development of a propagating flame front will most often occur at an earlier time after ignition than what is observed in the experiments, thus affecting the time-of-arrival of the peak overpressures. In addition, for the simulations presented here, modelled flame speeds are likely higher than those obtained in the experiments throughout the explosion event. The maximum overpressure observed in the experiments occurred at about 25 ms after the panels opened, while Flacs3 predicts that the maximum overpressure occurs around 30 ms after the panels open and Flacs2 around 22 ms. The vent panels in both Flacs2 and Flacs3 simulations open before the flame front reaches the pipe rack. At the time of maximum pressure in the container, the simulated flame front has propagated through the pipe rack.

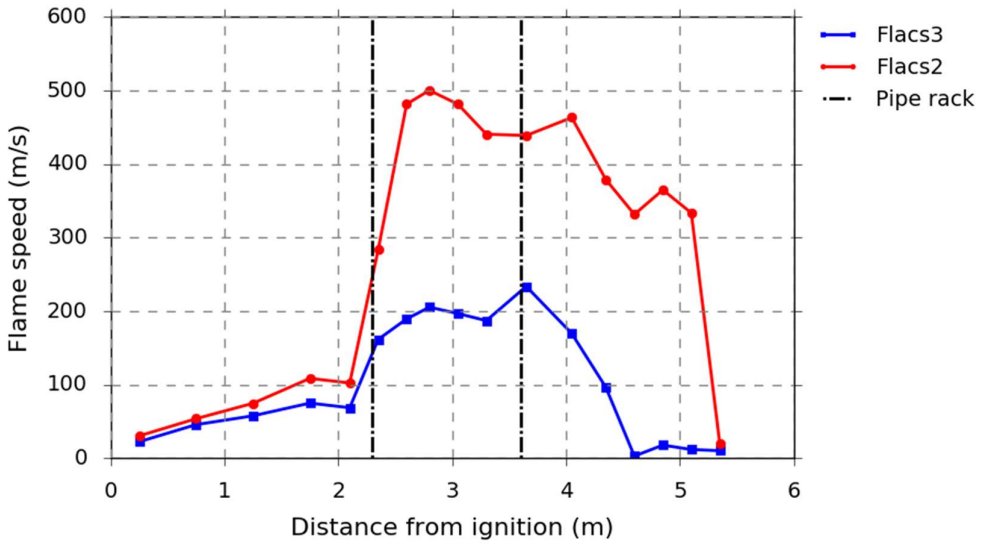

Figure 8. Simulated flame speed for Tests 60 and 61.

The measured maximum overpressures for homogeneous mixtures (tests 46 and 47 in Table 2) were about 1.8 times lower than for the inhomogeneous mixture tests with the same amount of fuel (tests 60 and 61). For Flacs3, the predicted maximum overpressure was 2.8 times lower and, for Flacs2, it was 11 times lower for the scenario with a homogeneous cloud than for the scenario with an inhomogeneous cloud. The significant over-prediction by Flacs2 for homogenous mixtures with about 24 vol.% hydrogen in air was discussed by Lakshmipathy *et al*. [23]. The hydrogen concentration near ignition for the stratified mixtures in this study exceeded 24 vol.%. This partly explains the significant over-prediction of pressures in simulations using Flacs2 in tests with inhomogeneous mixtures.

The stratified hydrogen mixture used as input to the explosion simulations (Figure 3 and Figure 4) had an overall higher concentration than that observed in the experiments. For lean mixtures, higher concentrations generally lead to higher peak pressures. To investigate this sensitivity, two user defined stratified clouds were used as input to the scenario in Test 60 with an overall difference of 2 vol.% hydrogen in air. The peak overpressure predicted by Flacs3 was reduced by 20 mbar when the overall hydrogen concentration was reduced. This suggest that the over-prediction of overpressure in Flacs3 is not significantly influenced by the over-predicted hydrogen concentrations.

6. CONCLUSION

A validation study for the in-house developed solver Flacs3 (used in FLACS *v11 beta*) was performed and compared to results from the Flacs2 solver (used in FLACS *v10.9*). Both model versions predict the release and dispersion of hydrogen inside 20-foot shipping containers with reasonable accuracy. Flacs2 significantly over-predicts the explosion pressure for ignited clouds generated by realistic hydrogen releases. The new combustion models in the Flacs3 solver improve the predictions. Overall, the peak overpressures predicted by Flacs3 were within a factor of two of the experimental results [24]. For the same average concentration of hydrogen in the container, the peak overpressure was higher for scenarios with stratified than for lean homogeneous mixtures, for both experiments and simulations. The hydrogen losses from the container prior to ignition in the experiments were unknown, and the overall fuel concentration was slightly over-predicted by the models. This likely had a limited effect on the subsequent over-prediction of explosion overpressure.

Some parameters in the sub-grid models are found using a parameter optimization routine [25] that includes a wide range of explosion experimental campaigns with different fuels. Hydrogen has not been included in the parameter optimization for Flacs2 or Flacs3.

ACKNOWLEDGEMENTS

The HySEA project received funding from the Fuel Cells and Hydrogen 2 Joint Undertaking (FCH 2 JU) under grant agreement No 671461. This Joint Undertaking received support from the European Union's Horizon 2020 research and innovation programme and the United Kingdom, Italy, Belgium and Norway.

REFERENCES

1. EN 14994:2007, Gas Explosion Venting Protective Systems, 2007 edition, BSI, UK, 2007.
2. NFPA 68, Standard on explosion protection by deflagration venting, 2013 edition, National Fire Protection Association, NFPA, Massachusetts, 2013.
3. Gexcon. FLACS User's Manual v10.9, Gexcon, Bergen, 2019.
4. Skjold, T., Hisken, H., Bernard, L., Mauri, L., Atanga, G., Lakshmipathy, S., Lucas, M., Carcassi, M., Schiavetti, M., Rao, V.C.M., Sinha, A., Tolias, I.C., Giannissi, S.G., Venetsanos, A.G., Stewart, J.R., Hansen, O.R., Kumar, C. and Krumenacker, L.L., Blind-prediction: estimating the consequences of vented hydrogen deflagrations for inhomogeneous mixtures in 20-foot ISO containers, Journal of Loss Prevention in the Process Industries, **61**, 2019, pp. 220-236.

5. Hjertager, B., Handbook of heat and mass transfer (Cheremisinoff, N.P. Eds.), Gulf Publishing Company, Houston, 1986, pp. 1303.
6. Patankar S.V. and Spalding, D.B., Heat exchangers: Design and theory sourcebook (Afgan, N. and Schlünder, E.U. Eds.), McGraw-Hill, New York, 1974, pp. 155.
7. Arntzen, B, Modelling of turbulence and combustion for simulation of gas explosions in complex geometries. PhD thesis, Department of Energy and Process Engineering, Norwegian University of Science and Technology, 1998, Norway.
8. Launder, B.E., and Spalding, D.B., The numerical computation of turbulent flows, *Computer Methods in Applied Mechanics and Engineering*, **3**, No 2, 1974, pp. 269–289
9. Bradley, D., Lawes, M., Liu, K. and Mansour, M., Measurements and correlations of turbulent burning velocities over wide ranges of fuels and elevated pressures, *Proceedings of the Combustion Institute*, **34**, No 1, 2013, pp. 1519-1526.
10. Bray, K.N.C., Studies of the turbulent burning velocity, *Proceedings: Mathematical and Physical Sciences*, **431**, No 1882, 1990, pp. 315-335.
11. Lipatnikov, A. and Chomiak, J., Turbulent flame speed and thickness: phenomenology, evaluation, and application in multi-dimensional simulations, *Progress in Energy and Combustion Science*, **28**, No 1, 2002, pp.1-73.
12. Bauwens, C. and Dorofeev, S., Experimental and numerical study on the effect of mixture composition on vented explosions, Proceedings of the Sixth International Seminar on Fire & Explosion Hazards, 11-16 April, 2011.
13. Keenan, J., Makarov, D., and Molkov, V., Rayleigh taylor instability: Modelling and effect on coherent deflagrations, *International Journal of Hydrogen Energy*, **39**, No 35, 2014, pp. 20467-20473.
14. Weller, H.G., Tabor, G., Gosman, A.D., and Fureby, C., Application of a flame-wrinkling LES combustion model to a turbulent mixing layer, *Symposium (International) on Combustion*, **27**, No 1, 1998, pp. 899-907
15. Puttock, J., Chakraborty, D., and Farmayan, W., Gas explosion modelling using PDRFoam, Tenth International Symposium on Hazards, Prevention, and Mitigation of Industrial Explosions, 10-14 June, 2014, Paper. 122.
16. Skjold, T., Vented hydrogen deflagrations in 20-foot ISO containers, Proceedings Twelfth International Symposium on Hazards, Prevention and Mitigation of Industrial Explosions, 12-17 August, 2018, pp. 823-846.
17. Skjold, T., Hisken, H., Lakshmipathy, S., Atanga, G., van Wingerden, M., Olsen, K.L, Holme, M.N., Turøy, N.M., Mykleby, M., and van Wingerden, K., Influence of congestion on vented hydrogen deflagrations in 20-foot ISO containers: homogeneous fuel-air mixtures, Twenty-Sixth International Colloquium on the Dynamics of Explosions and Reactive Systems (26 ICDERS), 2017.
18. Skjold, T., Hisken, H., Lakshmipathy, S., Atanga, G., Bernard, L., van Wingerden, M., Olsen, K.L., Holme, M.N., Turøy, N.M., Mykleby, M., van Wingerden, K., Vented hydrogen deflagrations in containers: Effect of congestion for homogeneous and inhomogeneous mixtures, International Journal of Hydrogen Energy, **44**, -No 17, 2019, pp. 8819-8832
19. Morse, A., Axisymmetric Turbulent Shear Flows with and without Swirl, PhD thesis, London University, 1977.
20. Pope, S., An Explanation of the Round Jet/Plane Jet Anomaly, AIAA Journal, **16**, No 3, 1978.
21. Middha, P., Development, use, and validation of the CFD tool FLACS for hydrogen safety studies, PhD thesis, Department of Physics and Technology, University of Bergen, Norway, 2010.
22. Hisken, H., Investigation of instability and turbulence effects on gas explosions: experiments and modelling, PhD thesis, University of Bergen, 2018.
23. Lakshmipathy, S., Skjold, T., Hisken, H. and Atanga, G., Consequence models for vented hydrogen deflagrations: CFD vs. engineering models. International Journal of Hydrogen Energy, **44**, No 17, 2019, p.p. 8699-8710

24. Hisken, H., Atanga, G., Skjold, T., Lakshmipathy, S., and Middha, P., Validating, documenting and qualifying models used for consequence assessment of hydrogen explosion scenarios. Eleventh International Symposium on Hazard, Prevention and Mitigation of Industrial Explosions, 24-29 July, 2016.
25. Both, A.-L., Gordon, A. and Hisken, H., CFD modelling of gas explosions: optimising sub-grid model parameters, *Journal of Loss Prevention in the Process Industries*, **60**, 2019, pp. 159-173.